Molecular Cell, Volume *80*

Supplemental Information

Nonstructural Protein 1 of SARS-CoV-2 Is a Potent Pathogenicity Factor Redirecting Host Protein Synthesis Machinery toward Viral RNA

Shuai Yuan, Lei Peng, Jonathan J. Park, Yingxia Hu, Swapnil C. Devarkar, Matthew B. Dong, Qi Shen, Shenping Wu, Sidi Chen, Ivan B. Lomakin, and Yong Xiong

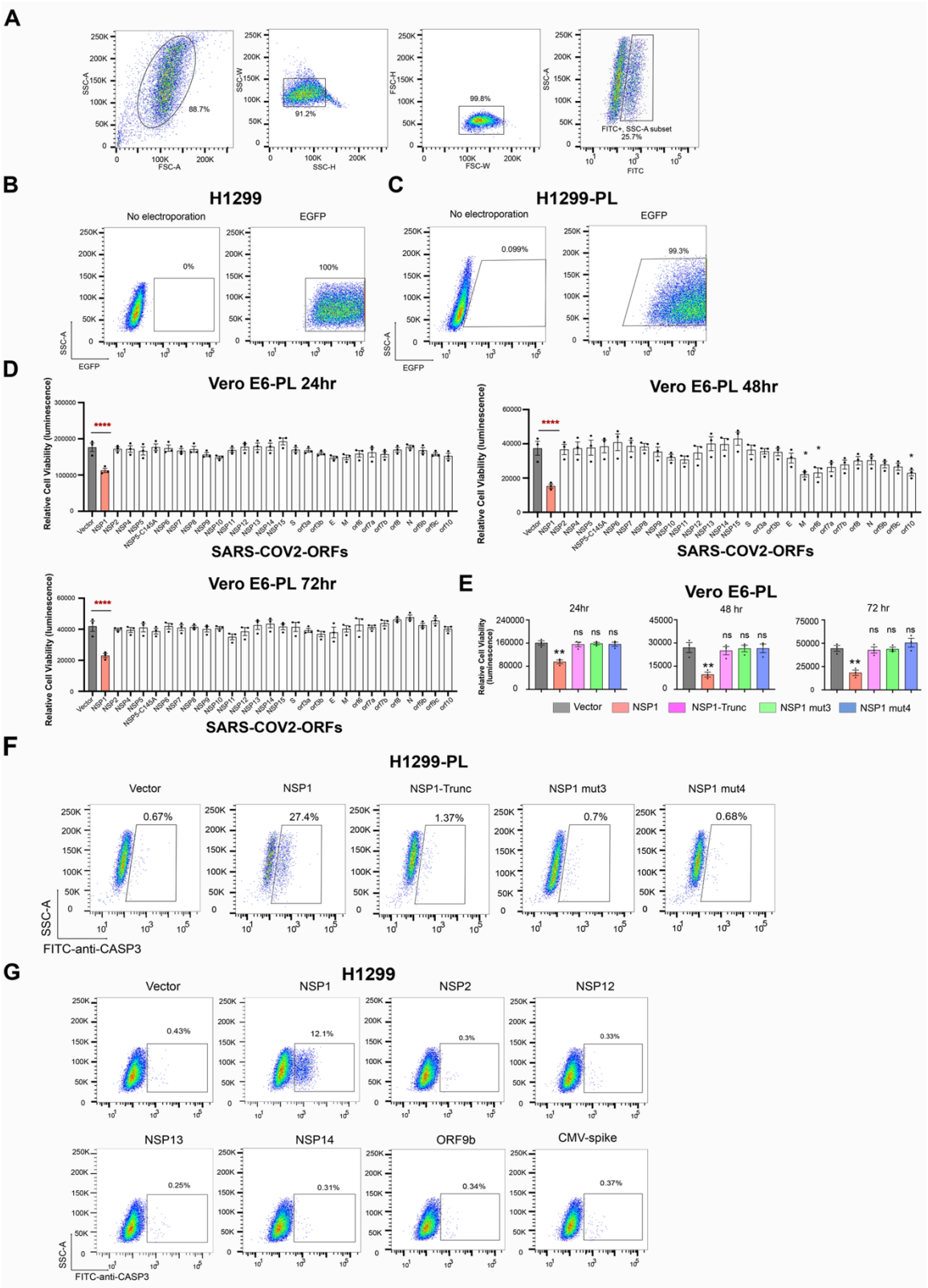

Figure S1. Flow cytometry analysis of cellular effects of SARS-CoV-2 ORFs, Nsp1, and Nsp1 mutants, Related to Figure 1.

(A) Diagram of example flow gating.
(B) Flow cytometry plots of GFP expression in H1299 cells, at 48 hours post ORF introduction.
(C) Flow cytometry plots of GFP expression in H1299-PL cells, at 48 hours post ORF introduction.
(D) Bar plot of firefly luciferase reporter measurement of viability effects of SARS-CoV-2 ORFs in Vero E6-PL cells, at 24, 48 and 72 hours post ORF introduction (n = 3 replicates).
(E) Bar plot of firefly luciferase reporter measurement of viability effects of Nsp1 and three Nsp1 mutants (truncation, mut3: R124S/K125E and mut4: N128S/K129E) in Vero E6-PL cells, at 24, 48 and 72 hours post ORF introduction (left, middle and right panels, respectively) (n = 3 replicates).
(F) Flow cytometry plots of apoptosis analysis of Nsp1 and three Nsp1 mutants (truncation, mut3: R124S/K125E and mut4: N128S/K129E) in H1299-PL cells, at 48 hours post ORF introduction. Percentage of apoptotic cells was gated as cleaved Caspase 3 positive cells.
(G) Flow cytometry plots of apoptosis analysis of several SARS-CoV-2 ORFs (Nsp1, Nsp2, Nsp12, Nsp13, Nsp14, Orf9b and Spike), at 48 hours post ORF introduction, in H1299 cells. Percentage of apoptotic cells was gated as cleaved Caspase 3 positive cells.

For all bar plots in this figure: Bar height represents mean value and error bars indicate standard error of the mean (sem). (n = 3 replicates for each group). Statistical significance was accessed by ordinary one-way ANOVA, with multiple group comparisons where each group was compared to empty vector control, with p-values subjected to multiple-testing correction by FDR method. (ns, not significant; * $p < 0.05$; ** $p < 0.01$; *** $p < 0.001$; **** $p < 0.0001$).

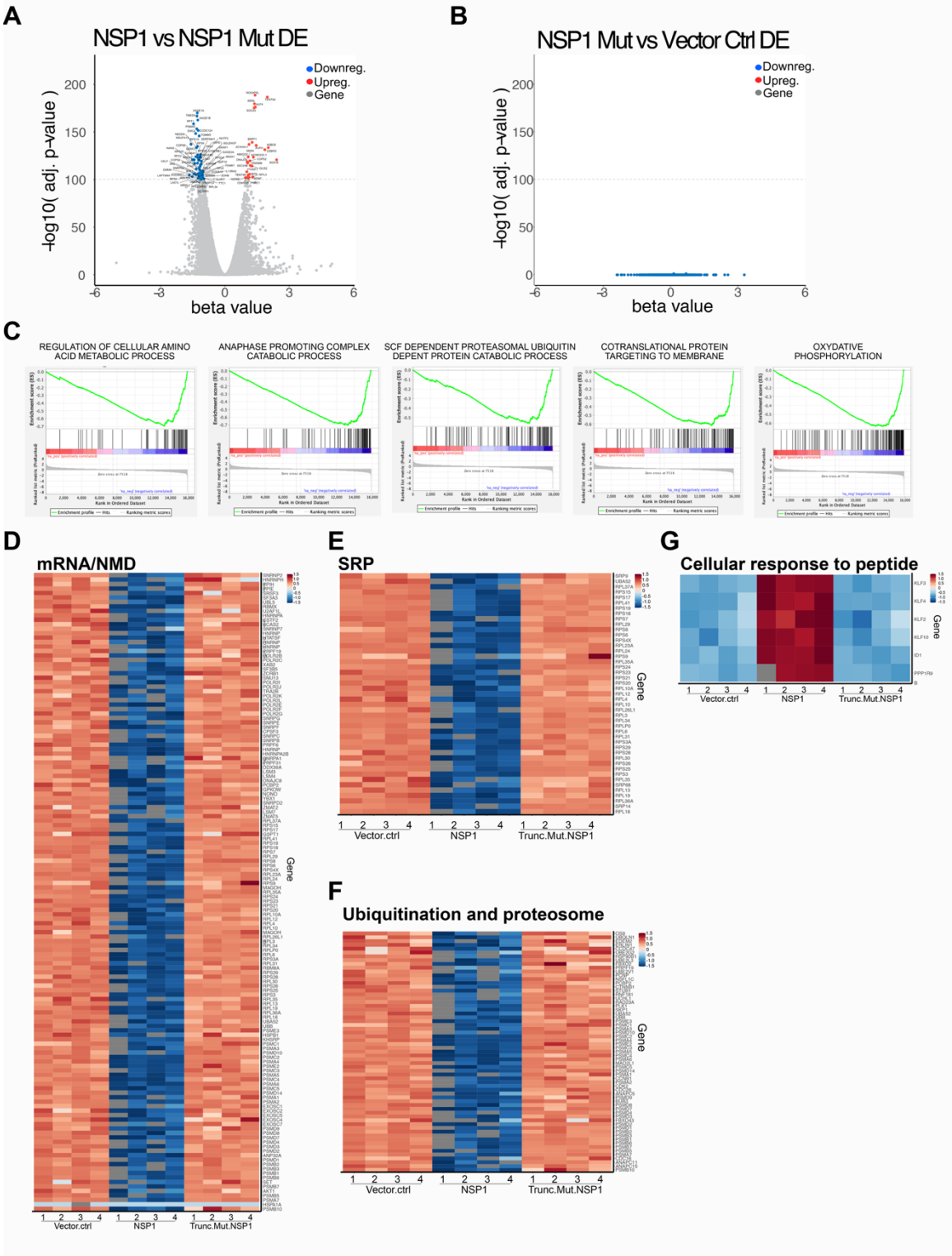

Figure S2. Additional differential expression and pathway analysis of H1299 Nsp1 mRNA-seq dataset, Related to Figures 2 and 3.

(A) Volcano plot of differential expression between of Nsp1 vs Nsp1 mutant electroporated cells. Genes highly differentially expressed (FDR adjusted

q value < 1e-100) are shown with gene names. Upregulated genes are shown in orange. Downregulated genes are shown in blue.

(B) Volcano plot of differential expression between of Nsp1 mutant vs Vector Control electroporated cells. As seen in the plot, no gene in the genome is differentially expressed between these two groups.

(C) Gene set enrichment plots of additional representative enriched pathways by GSEA.

(D) Heatmap of Nsp1 highly repressed genes (q < 1e-30) in the mRNA processing and nonsense-mediated decay processes.

(E) Heatmap of Nsp1 highly repressed genes (q < 1e-30) in the SRP proteins.

(F) Heatmap of Nsp1 highly repressed genes (q < 1e-30) in the ubiquitination and proteasome degradation processes.

(G) Heatmap of Nsp1 highly induced genes (q < 1e-30) in the cellular response to peptide processes.

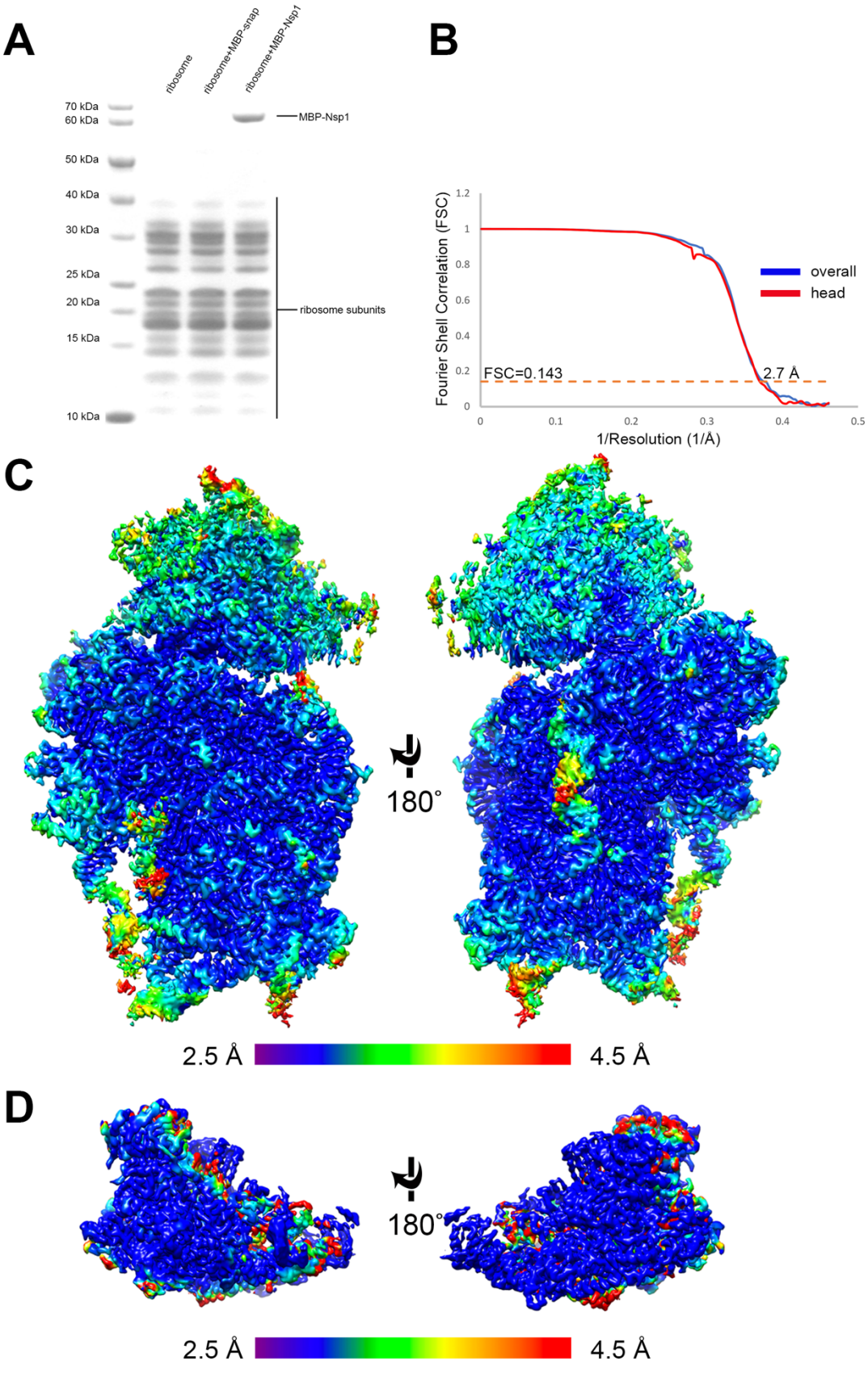
A
ribosome
ribosome+MBP-snap
ribosome+MBP-Nsp1
70 kDa
60 kDa
50 kDa
40 kDa
30 kDa
25 kDa
20 kDa
15 kDa
10 kDa
MBP-Nsp1
ribosome subunits
B
Fourier Shell Correlation (FSC)
1.2
1
0.8
0.6
0.4
0.2
0
0
0.1
0.2
0.3
0.4
0.5
1/Resolution (1/Å)
overall
head
FSC=0.143
2.7 Å
C
180°
2.5 Å
4.5 Å
D
180°
2.5 Å
4.5 Å

Figure S3. Data processing of Nsp1-40S ribosome complex cryo-EM dataset, Related to Figure 4.

(A) SDS-PAGE analysis of Nsp1 and 40S ribosome binding. Nsp1 is labeled with an MBP tag. MBP-snap was used as a negative control.

(B) FSC curves of the half-maps from gold standard refinement of the Nsp1-40S ribosome complex (blue) and masked local refinement of the head domain (red).

(C-D) Color coded local resolution estimation of the overall complex (**C**) and local-refined head domain (**D**).

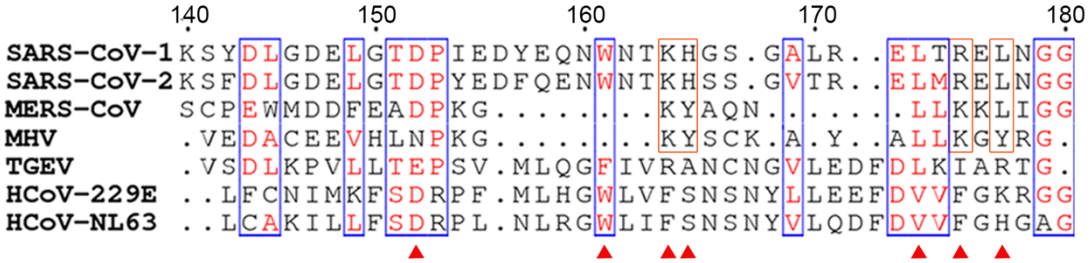

Figure S4. Alignment of the last 40 residues at Nsp1 C-terminus from beta-CoVs (SARS-CoV, SARS-CoV-2, MERS-CoV and MHV) and alpha-CoVs (TGEV, HCoV-229E and HCoV-NL63), Related to Figure 4.

Residues conserved in both alpha- and beta-CoVs are boxed in blue. Residues only conserved in beta-CoVs are with orange boxes. Conserved residues that mediate the interaction with the 40S are marked with red triangles.

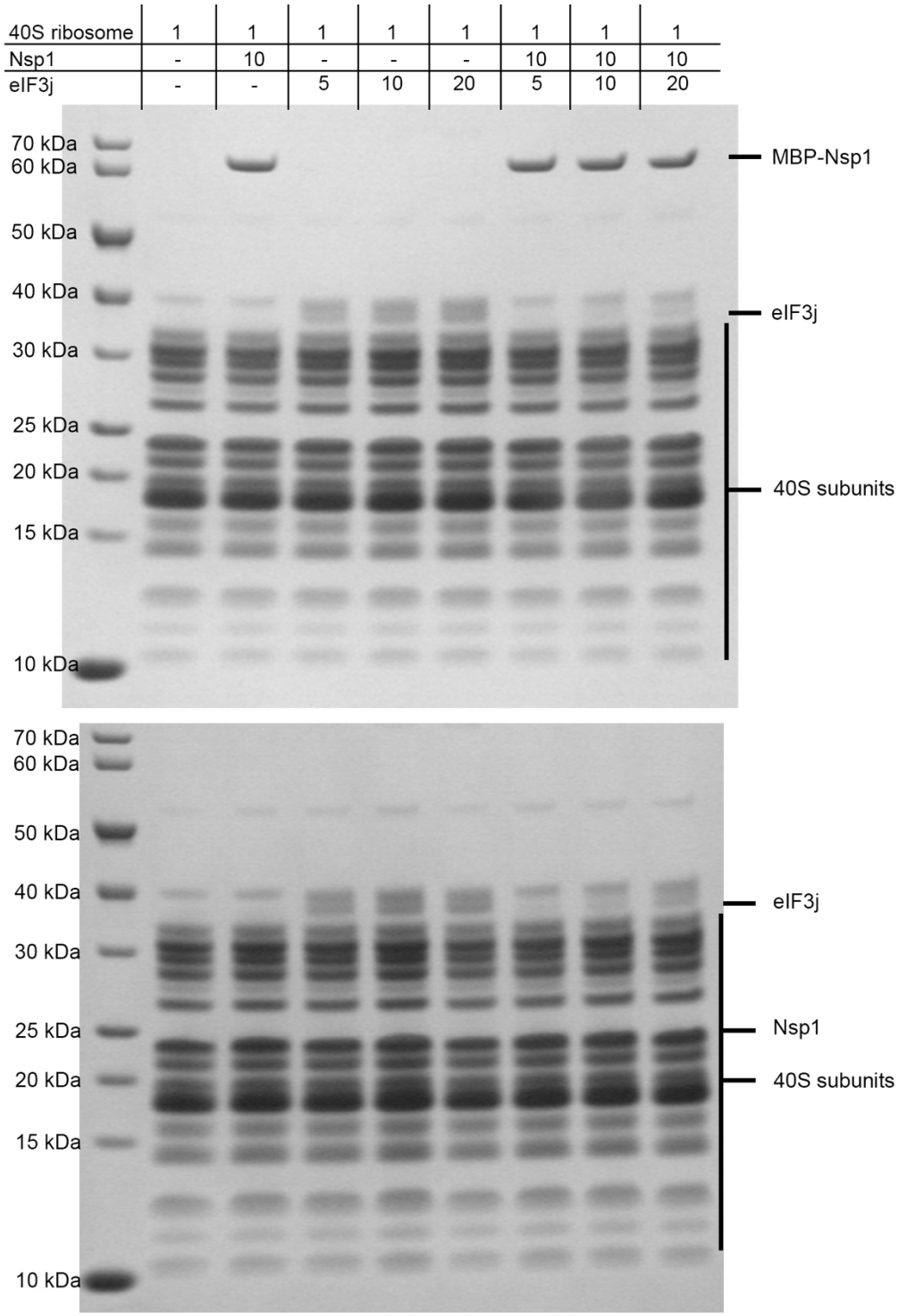

Figure S5. SDS-PAGE analysis of Nsp1 and eIF3j competition assay, Related to Figure 4.

Concentration ratios are shown in top table. Top gel: Assay with MBP-Nsp1. Bottom gel: Full-length Nsp1 without the MBP tag was used to exclude the tag effect.

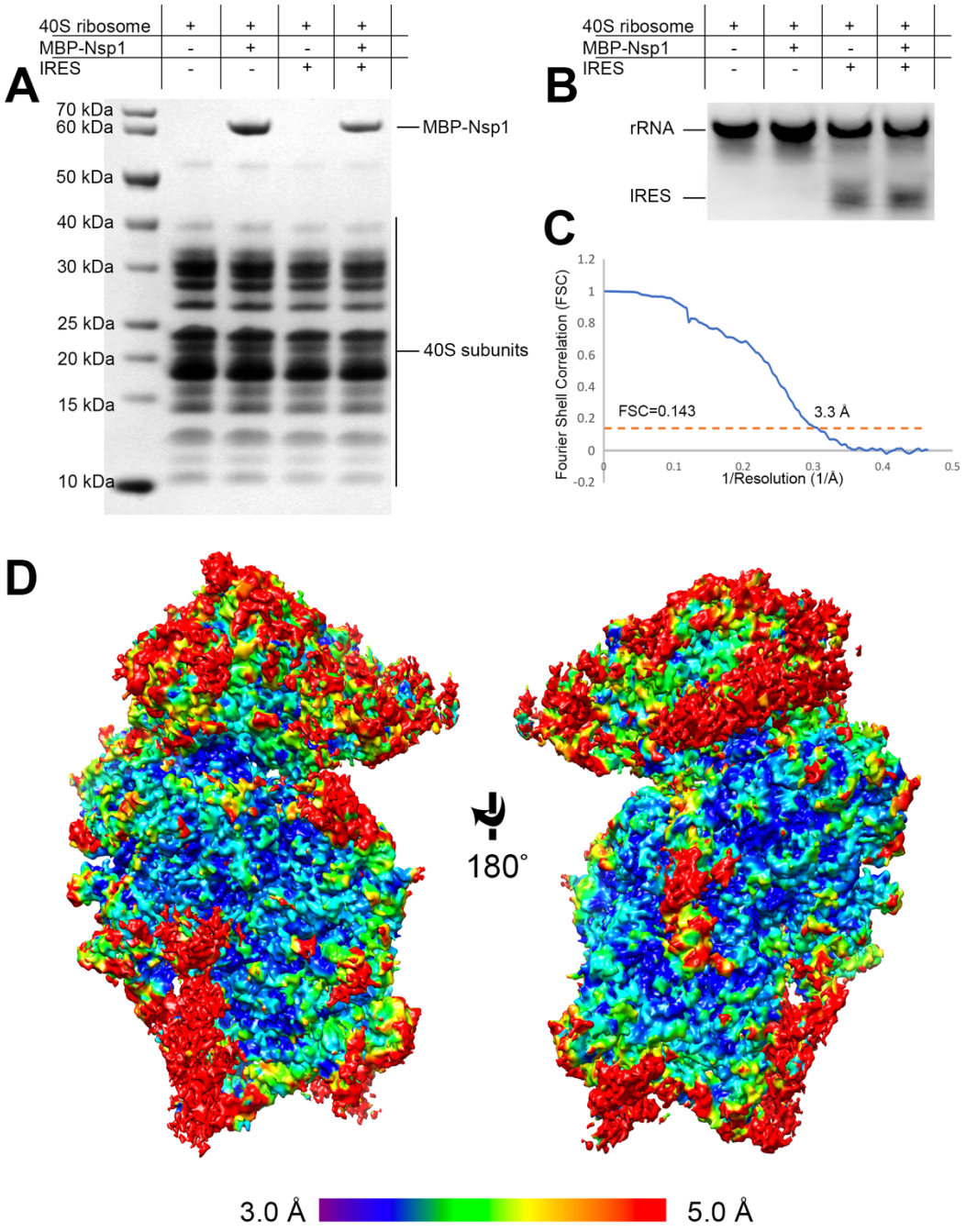

Figure S6. Data processing of Nsp1-40S-CrPV IRES complex cryo-EM dataset, Related to Figure 5.

(A-B) CrPV IRES and Nsp1 can bind to 40S ribosome simultaneously. SDS-PAGE. analysis **(A)** and RNA gel analysis **(B)** show the binding of Nsp1 and CrPV IRES.

(C) FSC curves of the half-maps from gold standard refinement of the Nsp1-40S-CrPV IRES complex.

(D) Color coded local resolution estimation of the complex.